

X-RAYS FROM THE VICINITY OF THE PROTOSTAR L1551 IRS 5: REFLECTION OR FAST SHOCKS?

JOHN BALLY,¹ ERIC FEIGELSON,² AND BO REIPURTH³

Received 2002 July 31; accepted 2002 October 31

ABSTRACT

We present new *Chandra X-Ray Observatory* observations of the L1551 molecular cloud in Taurus. We find a compact, but slightly resolved, X-ray source, displaced westward from the IRS 5 binary protostar by about 50–100 AU, which coincides with the base of the HH 154 protostellar jet. The column density of material lying in front of the X-ray source is more than an order of magnitude lower than the column density toward L1551 IRS 5. Thus, it is highly improbable that the X-rays come directly from the embedded protobinary. It is possible, however, that X-rays produced by one or both members of the IRS 5 binary escape through the outflow cavity and are scattered into the line of sight by a dense infalling envelope or material in the outflow. Constraints on the physical properties of the scattering medium are discussed. It is also possible that the X-rays are produced in situ by fast shocks at the base of the HH 154 jet. We consider several possible geometries for such shocks. The radiating plasma may be located behind standing shocks, where a wide-angle wind from one member of the IRS 5 binary is collimated into a jet, or behind shocks formed on the axis of the outflow, where winds from each member of the binary collide or where these winds impact a tilted circumbinary disk. To produce the observed X-ray luminosity and plasma temperature, shock velocities larger than 350 km s^{-1} are required, with a preshock hydrogen density of $(1\text{--}10) \times 10^3 \text{ cm}^{-3}$. The implied postshock cooling length is around 800 AU, close to the observed length of the bright near-infrared [Fe II] emission in the inner portion of the HH 154 jet.

Subject headings: ISM: individual (L1551) — ISM: jets and outflows — shock waves — stars: formation

1. INTRODUCTION

The ubiquitous protostellar outflows powered by low-mass young stars often take the form of highly collimated jets. However, several well-studied protostellar jets already have diameters of 100 AU at distances of only a few hundred AU from the source. Apparently, these outflows start as relatively wide angle winds, which become collimated into jets well away from the central engine (see, e.g., Raga, Mundt, & Ray 1991; Ray et al. 1996; Davis et al. 2002; Reipurth et al. 2002a). The nature of jet collimation remains an unsolved problem in star formation. If a solution to this problem can be found for Herbig-Haro jets, it may shed light on the production of jets in other astrophysical systems.

In most models, outflows are launched from the inner edge of an accretion disk or from the stellar magnetosphere within an AU of the central star. The mechanism that collimates such winds into jets may involve magnetic hoop stress, the ram pressure of an accreting envelope, or interactions with a dense surrounding medium. Part of the difficulty in diagnosing the collimation mechanism is that circumstellar obscuration and scattered light often hides the region where the relevant interactions take place. In this paper, we present *Chandra* observations of the binary protostar L1551 IRS 5 and its twin jets. These data probe the

region where the HH 154 jet emerging from this system may be collimated.

The dark cloud L1551, located at a distance of 140 pc in Taurus, is one of the nearest sites of ongoing low-mass star formation. This $40 M_{\odot}$ cloud has given birth to at least a dozen stars, several of which are actively driving jets and outflows into the surrounding medium. The most luminous source in the cloud is L1551 IRS 5 ($L \approx 40 L_{\odot}$), which was recently discovered to be a 40 AU separation protobinary (Rodríguez et al. 1998). The source is deeply embedded and is obscured by about 150 mag at visual wavelengths (see, e.g., White et al. 2000), implying a foreground column density $\log N_{\text{H}} \approx 10^{23.5} \text{ cm}^{-2}$. L1551 IRS 5 powers a small Herbig-Haro jet, known as HH 154 (Fridlund & Liseau 1998), and one of the first recognized bipolar molecular outflows (Snell, Loren, & Plambeck 1980; Moriarty-Schieven & Snell 1988). The blueshifted southwestern and redshifted northeastern lobes of the L1551 IRS 5 molecular outflow contain dozens of shocks visible at visual wavelengths and cataloged as Herbig-Haro objects (HH 28, 29, 258, 259, 262, and 286; see Devine, Reipurth, & Bally 1999; Reipurth 1999).⁴ At least five other young stellar objects (YSOs) are simultaneously powering additional jets and outflows in L1551. These include the spectacular HH 30 jet and its embedded source, the classical T Tauri stars HL and XZ Tau and their associated outflows HH 266 and 153, and LkH α 358 and the flow HH 265 located north of IRS 5. In addition, the source L1551 NE, located about $90''$ from IRS 5, drives a highly collimated jet, HH 254 (Reipurth et al. 2000), which powers HH 29, the brightest HH object in L1551 (Devine et al. 1999, 2000). Thus, the L1551 cloud is one of the most active

¹ Center for Astrophysics and Space Astronomy, University of Colorado, CB 389, Boulder, CO 80309; bally@casa.colorado.edu.

² Department of Astronomy and Astrophysics, Pennsylvania State University, 525 Davey Laboratory, University Park, PA 16802; edf@astro.psu.edu.

³ Institute for Astronomy, University of Hawaii, 2680 Woodlawn Drive, Honolulu, HI 96822; reipurth@ifa.hawaii.edu.

⁴ Reipurth (1999) is available at <http://www2.ifa.hawaii.edu/CSPF> (in “catalogs” menu).

sites of nearby star formation and contains the closest interstellar shocks bright at visual wavelengths.

The L1551 cloud has played an important early role in the study of X-ray emission from pre-main-sequence stars. It was the discovery site of the first X-ray-bright “weak-lined” T Tauri stars (Feigelson & DeCampli 1981; Feigelson & Kriss 1981). One of these stars, V826 Tau, emerged as the first known double-lined spectroscopic binary T Tauri star (Mundt et al. 1983; Reipurth et al. 1990). Carkner et al. (1996) present a thorough X-ray study of the cloud, using the *ROSAT* and *ASCA* satellites. Seven well-known and seven potential new T Tauri stars were detected with a sensitivity of $L_X \simeq 3 \times 10^{28}$ ergs s^{-1} (assuming negligible absorption), plus a score of unrelated sources, such as foreground members of the Hyades. None of the embedded protostars were detected with upper limits of $L_X < 3 \times 10^{30}$ ergs s^{-1} in the 0.5–10 keV band, assuming line-of-sight absorption from a column density $\log N_H = 23.0$ cm^{-2} .

Recently, Favata et al. (2002) report a faint X-ray source near the L1551 IRS 5 binary, based on a $\simeq 50$ ks observation of the cloud with the *XMM-Newton* observatory. They detected 42 X-ray photons with $L_X \simeq 3 \times 10^{29}$ ergs s^{-1} within the $\simeq 14''$ FWHP point-spread function (PSF). The X-ray photon energies range from 0.5 to 2 keV and may arise from a plasma with $kT \sim 4$ keV suffering moderate absorption, with $\log N_H \simeq 22.1$ cm^{-2} . Favata et al. interpret this as shocked plasma from the working surface knot D in the 200–300 $km s^{-1}$ HH 154 outflow. Two harder sources (apparently background) were also detected 1.7 and 2.5 west of IRS 5 in the extended blueshifted lobe of the outflow.

In this paper, new, higher angular resolution X-ray observations are presented, based on data from the *Chandra X-Ray Observatory*. The new data demonstrate that X-ray emission from the vicinity of L1551 IRS 5 originates at the base of the HH 154 jet and *not* from its working surface, knot D.

2. OBSERVATIONS AND ANALYSIS

2.1. *Chandra* Data

L1551 was observed with the imaging array of the Advanced CCD Imaging Spectrometer (ACIS-I) on board *Chandra*; the satellite and instrument are described by Weisskopf et al. (2002). The array subtends about $17' \times 17'$, with a nominal J2000.0 aim point at $(04^h 31^m 32.7^s, 18^\circ 08' 08'')$ and roll angle $101^\circ 8'$ east of north (see Fig. 1). The effective exposure time was 78.93 ks (21.9 hr), starting 2001 July 23.22 UT. The data are continuous except for minor dropouts of two or three 3.2 s frames in each CCD. After the data-cleaning operations (see below), the detector background was low, at 3.8×10^{-3} counts $arcsec^{-2}$, and exhibited no temporal variations greater than $\pm 5\%$. This indicates quiet space weather conditions in the spacecraft environs during the observation.

Data analysis generally followed procedures described in detail by Feigelson et al. (2002), with updates outlined by Getman et al. (2002). We start with level 1 ACIS events provided by the *Chandra* X-Ray Center. The data were reprojected to remove $\pm 0''.25$ randomization and to apply a new detector geometry file. Events with CCD grades, status bits, and energies inconsistent with real X-ray events were removed, and an array exposure map was produced. Event

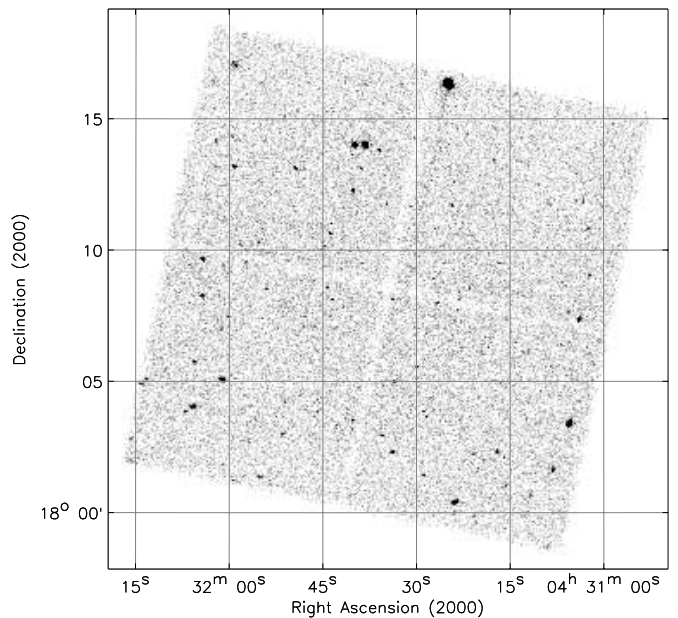


FIG. 1.—*Chandra* ACIS-I L1551 image

energies and grades were corrected for the degradation due to charge transfer inefficiency induced by particle irradiation of the CCDs early in the *Chandra* mission, following the procedures of Townsley et al. (2000, 2002). Repeated events, either caused by cosmic-ray afterglows or from astronomical sources, were removed for source detection but were retained for source analysis. The data set at this point resembles the level 2 event list provided by the mid-2001 standard *Chandra* pipeline reduction system, but with somewhat improved sensitivity and event energies due to the more sophisticated treatment of charge transfer inefficiency and improved locations due to the new detector geometry map.

Source detection was performed on the images in the full *Chandra* band (0.5–8 keV) using the wavelet transform algorithm described by Freeman et al. (2002) at a range of spatial scales. We used a source significance threshold of $P = 3 \times 10^{-5}$, which is more sensitive than the recommended value $P = 1 \times 10^{-6}$ and thus gives a considerable number of spurious, as well as real, faint sources. The purpose of delving into the noise of the ACIS image is to uncover the faintest possible sources for comparison with optical and near-infrared stellar catalogs. Getman et al. (2002) show for a 38 ks exposure of the NGC 1333 molecular cloud that sources as faint as 3 ACIS counts have convincing young stellar counterparts. The *wavdetect* sources were then examined visually on the X-ray image, and the source list was improved by the removal of likely spurious faint triggers and the addition of possible faint sources missed by the algorithm and sources missed because of close proximity to another source. These sources are listed in Table 1, with wavelet detection positions corrected to the *Hipparcos* reference frame as described in § 2.2.

Events were extracted from the ACIS data from a polygonal region around each source centroid scaled to the local PSF shape. Table 1 gives the background-corrected source counts and the area of the extraction region in $0''.5 \times 0''.5$ pixels. Recognizing that our source detection procedure

TABLE 1
Chandra X-RAY SOURCES IN L1551

Source	α (J2000.0)	δ (J2000.0)	Counts	Area ($0''.5 \times 0''.5$ pixels)
1.....	4 31 02.51	18 08 59.7	28	501
2.....	4 31 02.68	18 10 46.0	35	577
3.....	4 31 04.17	18 07 18.9	209	447
4.....	4 31 05.77	18 03 21.0	1003	694
5.....	4 31 05.94	18 07 36.2	23	361
6.....	4 31 08.40	18 01 36.0	71	870
7.....	4 31 09.36	18 08 40.5	36	2202
8.....	4 31 11.98	18 00 40.6	33	951
9.....	4 31 15.89	18 00 57.7	28	703
10.....	4 31 17.11	18 09 26.7	19	86
11.....	4 31 17.28	18 02 16.1	46	394
12.....	4 31 17.78	18 13 24.1	18	320
13.....	4 31 18.74	18 06 14.0	6 ^a	80
14.....	4 31 20.37	18 01 38.8	10 ^a	434
15.....	4 31 21.11	18 02 12.0	22	326
16.....	4 31 23.35	18 08 04.2	53	52
17.....	4 31 23.78	18 07 39.9	5 ^a	50
18.....	4 31 24.06	18 00 21.4	285	666
19.....	4 31 24.13	18 12 32.7	13	148
20.....	4 31 24.56	18 11 39.5	51	89
21.....	4 31 25.10	18 16 17.2	11451	1245
22.....	4 31 26.89	18 07 55.7	118	42
23.....	4 31 27.22	18 10 46.7	20	65
24.....	4 31 27.44	18 08 50.7	11	87
25.....	4 31 29.05	18 03 47.7	14	103
26.....	4 31 29.10	18 01 22.8	39	399
27.....	4 31 30.17	18 05 31.2	28	59
28.....	4 31 31.23	18 11 37.6	10	96
29.....	4 31 33.76	18 04 56.8	24	72
30.....	4 31 33.98	18 02 16.1	65	252
31.....	4 31 34.10	18 08 04.9	60	37
32.....	4 31 34.95	18 11 41.8	13	76
33.....	4 31 35.66	18 02 53.5	37	187
34.....	4 31 36.15	18 13 44.1	60	237
35.....	4 31 38.41	18 13 57.9	1983	277
36.....	4 31 39.04	18 13 03.5	14	174
37.....	4 31 40.09	18 13 57.5	1907	287
38.....	4 31 40.33	18 12 12.5	244	116
39.....	4 31 40.44	18 03 27.7	40	158
40.....	4 31 42.95	18 03 17.2	23	199
41.....	4 31 43.66	18 08 05.5	25	58
42.....	4 31 44.01	18 10 34.9	71	91
43.....	4 31 44.47	18 08 32.0	40	63
44.....	4 31 44.86	18 10 05.5	48	89
45.....	4 31 46.01	18 03 48.9	16	182
46.....	4 31 49.52	18 13 03.4	57	305
47.....	4 31 51.58	18 02 56.1	34	390
48.....	4 31 54.13	18 08 28.2	22	167
49.....	4 31 55.20	18 01 19.0	53	903
50.....	4 31 55.46	18 10 14.7	21	256
51.....	4 31 57.53	18 09 29.4	18	290
52.....	4 31 58.44	18 10 10.0	25	363
53.....	4 31 59.33	18 16 59.4	73	695
54.....	4 31 59.34	18 13 07.7	101	1912
55.....	4 31 59.82	18 14 16.4	31	976
56.....	4 32 00.33	18 07 24.0	18	358
57.....	4 32 01.25	18 05 01.2	213	507
58.....	4 32 01.46	18 06 59.7	22	419
59.....	4 32 02.24	18 14 04.4	38	1139
60.....	4 32 02.66	18 15 21.8	46	2229
61.....	4 32 04.37	18 09 36.4	76	649
62.....	4 32 04.49	18 08 12.8	74	574
63.....	4 32 05.74	18 05 40.7	49	713
64.....	4 32 05.97	18 03 59.2	127	956

TABLE 1—*Continued*

Source	α (J2000.0)	δ (J2000.0)	Counts	Area ($0''.5 \times 0''.5$ pixels)
65.....	4 32 07.20	18 03 46.8	38	1103
66.....	4 32 13.31	18 05 00.3	50	1890
67.....	4 32 14.12	18 04 51.4	50	1948
68.....	4 32 15.77	18 02 44.1	41	2553
69.....	4 32 15.90	18 01 57.8	57	2817

NOTE.—Units of right ascension are hours, minutes, and seconds, and units of declination are degrees, arcminutes, and arcseconds.

^a The X-ray source is only marginally detected. It is retained in this table because of its possible association with an optical counterpart.

may produce some spurious faint sources, we follow Feigelson et al. (2002; see their eq. [5]) by adopting a limit of source counts $C_{\text{lim}} = 5 + 0.28\theta^2$, where θ is the off-axis angle in arcminutes, above which we are confident that the source detection procedure is complete and source existence is reliable. Sources falling below this limit are omitted, except for three (sources 13, 14, and 17) that coincide with counterparts at other wavelengths.

Visual wavelength images used in this analysis were obtained on 2001 October 12 at the f/3.1 prime focus of the 4 m Mayall reflector located on Kitt Peak near Tucson, Arizona, using the 8192×8192 pixel MOSAIC imager, which utilizes a 2×4 array of 2048×4096 pixel-thinned and back-side-illuminated SITE CCDs with $15 \mu\text{m}$ pixels. This camera provides a $35'.4$ field of view with a scale of $0''.258$ pixel⁻¹. Narrowband images were obtained through matched interference filters with 80 \AA passbands that transmit the 6563 \AA H α and the $(6717+6731) \text{ \AA}$ [S II] lines. A set of five exposures, each with a duration of 400 s, was obtained in a dither pattern that guarantees that no field point falls into the inter-CCD gaps in more than two images. A 30 s exposure in the broadband SDSS i' filter was used to measure the continuum emission. The data were reduced with the MSCRED package in IRAF. Astrometric coordinates were determined by registering several thousand stars in the image to their USNO-A2.0 catalog positions. After high proper motion stars are rejected, the estimated error in the coordinates is about $0''.3$.

Table 2 lists X-ray sources with stellar counterparts and those associated with previously known young stars. In this paper, we concentrate on the interpretation of X-ray emission associated with the protobinary L1551 IRS 5 and its twin jets, HH 154 (source 31). A detailed discussion of the other X-ray sources in L1551 will be presented in a separate paper. From *Chandra* measurements of the extragalactic $\log N - \log S$ count distribution, we estimate that roughly 20–30 of the sources above the completeness limit C_{lim} are probably background sources (Campana et al. 2001a, 2001b). But this value is quite uncertain because of the spatially variable extinction of the softer X-rays by the L1551 molecular cloud.

2.2. Astrometry

Astrometric alignment of ACIS images of rich young stellar clusters to the *Hipparcos* reference frame can often be made to $\pm 0''.1$ accuracy (see, e.g., Feigelson et al. 2002). But this is more difficult for the L1551 field, because fewer X-ray sources are present and, by happenstance, the strongest

TABLE 2
X-RAY SOURCES WITH OPTICAL OR RADIO COUNTERPARTS

SOURCE	<i>Chandra</i> COORDINATES		OPTICAL COORDINATES ^a		COUNTS	COMMENTS
	α (J2000.0)	δ (J2000.0)	α (J2000.0)	δ (J2000.0)		
4.....	4 31 05.77	18 03 21.0	4 31 05.84	18 03 21.1	1003	$m(R) = 15$ star in HH 28
13.....	4 31 18.74	18 06 14.0	4 31 18.4	18 06 16	6	In HH 264 ^b
14.....	4 31 20.37	18 01 38.8	4 31 20.33	18 01 38.5	10	$m(R) = 16.9$ star
17.....	4 31 23.78	18 07 39.9	4 31 23.4	18 07 48	5	In HH 263 ^b
18.....	4 31 24.06	18 00 21.4	4 31 24.06	18 00 21.6	285	Faint star
21.....	4 31 25.10	18 16 17.2	4 31 25.14	18 16 16.8	11451	$m(R) = 19.9$ HD 285845
26.....	4 31 29.10	18 01 22.8	4 31 29.11	18 01 23.7	39	Very faint star
31.....	4 31 34.10	18 08 04.9	4 31 34.13	18 08 05.2	60	L1551 IRS 5A ^c
			4 31 34.13	18 08 04.8	...	L1551 IRS 5B ^c
34.....	4 31 36.15	18 13 44.1	4 28 41.00	18 07 18.0	60	LkH α 358 ^d
35.....	4 31 38.41	18 13 57.9	4 31 38.43	18 13 59.0	1983	HL Tau ^e
37.....	4 31 40.09	18 13 57.5	4 31 40.02	18 13 57.8	1907	XZ Tau ^e
43.....	4 31 44.47	18 08 32.0	4 31 44.50	18 08 31.7	40	L1551 NE A ^d
			4 31 44.47	18 08 31.9	40	L1551 NE B ^d
49.....	4 31 55.20	18 01 19.0	4 31 55.17	18 01 19.1	53	Faint star
57.....	4 32 01.25	18 05 01.2	4 32 01.24	18 05 01.1	213	Faint star

NOTE.—Units of right ascension are hours, minutes, and seconds, and units of declination are degrees, arcminutes, and arcseconds.

^a Unless otherwise noted, optical coordinates are from the 2001 MOSAIC CCD image, which is referenced to the USNO-A2.0 catalog.

^b Optical coordinates from Reipurth 1999. These HH objects are large, with diameters of tens of arcseconds.

^c Radio coordinates are from Rodríguez et al. 1998.

^d Radio positions from Reipurth et al. 2002b.

^e Gezari, Pitts, & Schmitz 1999; radio positions from Wendker 1995.

sources lie far off-axis, where the *Chandra* PSF is broad and distorted.

The 2001 epoch narrowband images of L1551 obtained at KPNO were used to register the ACIS data to the optical reference frame. Eight X-ray sources in Tables 1 and 2 (ACIS sources 4, 14, 18, 21, 26, 37, 49, and 57) that have unambiguous stellar counterparts in the KPNO images were used to estimate the offset between the X-ray and optical coordinates. The brightest ACIS source, associated with the $V = 10$ mag G6 star HD 285845 (=Tyc 1269-469-1; source 21), is saturated in the optical image. The intersection of the diffraction spikes was used to mark its position. The bright ACIS source (source 37 in Tables 1 and 2), 6' north of the aim point, is associated with the young star XZ Tau, which has a well-determined optical position. However, the adjacent young stars, HL Tau (source 35) and LkH α 358 (source 34), do not have well-determined optical positions, since their emission at visual wavelengths is dominated by reflection nebulae. The young binary stars L1551 IRS 5 (source 31) and L1551 NE (source 43) only have positions determined at infrared and radio wavelengths. Thus, these four sources (31, 34, 35, and 43) were not used for astrometry.

The nominal ACIS positions were found to be offset from the optical by 0".53 to the west and 1".39 to the north with respect to the optical counterparts. The rms error in this offset is about 0".6 in R.A. and 0".4 in decl. Tables 1 and 2 give the X-ray source positions corrected to the optical reference frame. Since both the optical and X-ray images were obtained within 3 months of each other, registration should be excellent, as proper motions are too small to produce measurable displacements over such a short time interval.

3. PROTOSTELLAR AND HERBIG-HARO JET X-RAY EMISSION

3.1. L1551 IRS 5

The main observational result of this study is that the X-ray emission from the vicinity of L1551 IRS 5 discovered by Favata et al. (2002) arises from a compact source located at the base of the HH 154 protostellar jet.

As shown in Table 2 and Figure 2, source 31 is located at about 0".5–1" west of the VLA source position. The biggest uncertainty in this statement is the registration of the X-ray/optical coordinates with the radio reference frame.

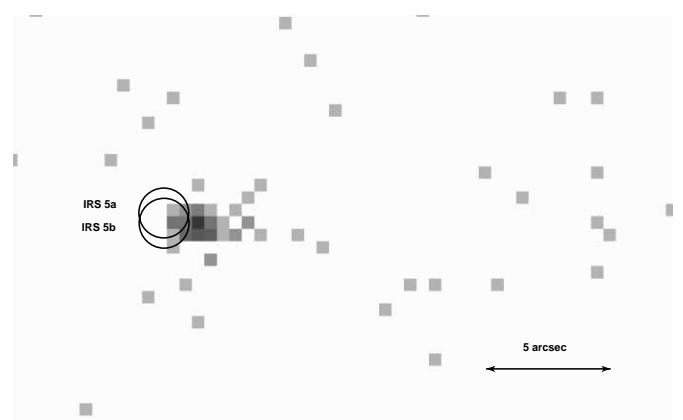


FIG. 2.—Close-up view of the X-ray source near L1551 IRS 5 (peak = 13 counts pixel⁻¹). The image is displayed with a scale of 0".5 pixel⁻¹. The protostellar positions from Rodríguez et al. (1998) are shown.

We estimate that the uncertainty in the registration of these frames is about $0''.5$, from the coincidence of the X-ray and radio position of L1551 NE (see below), the X-ray and optical positions of HL and XZ Tau, and a separate estimate of the offsets between the optical/NIR and radio reference frames. The published infrared position for IRS 5, which is referenced to stars, is about $0''.5$ or more east of ACIS source 31.

Figure 2 shows that source 31 is slightly extended along the HH 154 axis. Since source 31 is located only $21''$ from the aim point, the X-ray PSF is very clean at this location. In addition, as listed in Table 1, 60 counts were detected in a $3''.59$ radius circle centered on source 31 in the 0.5–8 keV band. However, only 47 counts were extracted from a circular region with a $1''.7$ radius centered on the position of this source. This latter extraction radius is chosen to include 95% of the events from the local PSF. Less than 1 count is expected from the detector background. The arrival times show no evidence of variability from visual examination and use of the Kolmogorov-Smirnov test.

The photon energies are strongly concentrated in the 1–2 keV range. Spectral fitting is performed by least-squares minimization to a MEKAL (Mewe, Lemen, & van den Oord 1986) optically thin spectral plasma at a single temperature, subject to interstellar absorption using Morrison & McCammon (1983) cross sections. The spectral calibration (arf and rmf files) take into account the correction to the charge transfer inefficiency and the recently observed degradation in low-energy response due to deposition on the detector, as well as the usual mirror and detector efficiency characteristics.

The data are well fitted with models ranging from $N_{\text{H}} = 0 \text{ cm}^{-2}$ with a plasma energy of $kT = 4 \pm 1 \text{ keV}$ ($\chi^2_{\nu} = 0.7$) to $N_{\text{H}} = 1 \times 10^{22} \text{ cm}^{-2}$ with $kT = 1.0 \pm 0.3 \text{ keV}$ ($\chi^2_{\nu} = 1.0$). However, absorption due to hydrogen column densities higher than 2×10^{22} does not give successful fits. We conclude from the spectral analysis that $N_{\text{H}} < 2 \times 10^{22} \text{ cm}^{-2}$ and $0.5 \text{ keV} < kT < 5 \text{ keV}$.

For an intermediate value of $N_{\text{H}} = 1 \times 10^{22}$ and a distance of 140 pc, the broadband X-ray luminosity is $L_{\text{X}} = 3 \times 10^{28} \text{ ergs s}^{-1}$ in the 0.5–8 keV range, roughly equally divided between the soft (0.5–2 keV) and hard (2–8 keV) bands. For the extended source (60 photons), this N_{H} implies $L_{\text{X}} = 4 \times 10^{28} \text{ ergs s}^{-1}$. We adopt this luminosity for the discussion below.

Favata et al. (2002) detected X-ray emission from the L1551 IRS 5 region, using data from *XMM-Newton*, which has a much larger PSF than *Chandra*. They argue that the source arises from the $\text{H}\alpha$ -bright knot D $10''$ west of IRS 5. However, the centroid of their 42 X-ray photons lies $3''.0 \pm 2''$ southwest of IRS 5 (where the error here is the field boresight uncertainty and does not include dispersion from the PSF), closer to the protostar than the knot. Favata et al. (2002) applied a shock model to this knot, predicting a post-shock temperature around $T \simeq 0.7 \text{ MK}$, not consistent with their observed temperature $4 \pm 2.5 \text{ MK}$. It also would require that the X-ray luminosity be an order of magnitude higher than the $\text{H}\alpha$ emission from the knot. As discussed above, the *Chandra* ACIS spectral fits are consistent with a temperature of 6–60 MK and $N_{\text{H}} < 10^{22.3} \text{ cm}^{-2}$; we adopt a value of 10 MK for the discussion below.

Our *Chandra* data indicate that the *XMM-Newton* source arises from either the protostar IRS 5 or its immediate vicinity. The difference between the *Chandra* and *XMM* position

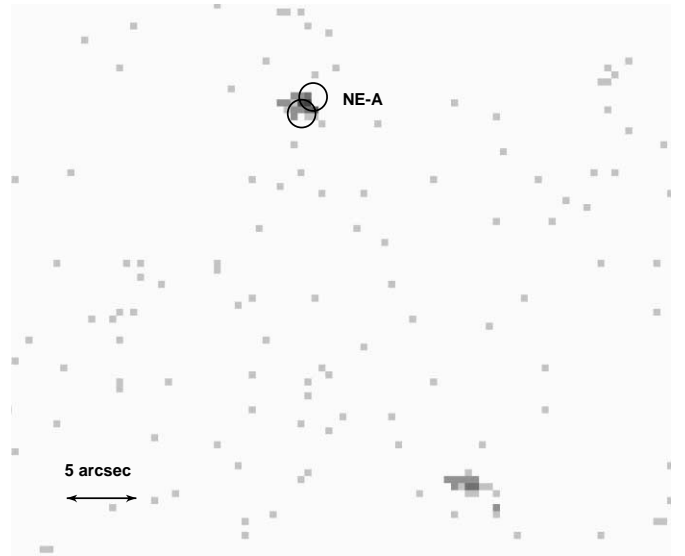


FIG. 3.—Close-up view of the X-ray source near L1551 NE (peak = 6 counts pixel $^{-1}$). The panel includes a nearby source to compare PSF shapes. The image is displayed with a scale of $0''.5$ pixel $^{-1}$. The protostellar positions from Reipurth et al. (2002b) are shown.

is not strongly affected by the uncertain absorption toward the source, as both observations refer to the same 0.5–5 keV band. The difficulty with a protostellar origin, as pointed out by Favata et al. (2002), is that the assumed visual extinction of roughly 150 mag corresponds to an absorption around $\log N_{\text{H}} \simeq 23.5 \text{ cm}^{-2}$, far above the values $\log N_{\text{H}} = 22.1 \pm 0.1 \text{ cm}^{-2}$ inferred from the *XMM-Newton* spectrum or $\log N_{\text{H}} < 22.3 \text{ cm}^{-2}$ constrained by our *Chandra* spectrum. This model is viable only if the X-ray emission arises from a region with much less absorption than the bulk of the protostellar infrared emission.

3.2. L1551 NE

This source (43) lies several arcminutes off-axis, where the *Chandra* PSF is no longer optimal. Examination of the source morphology shows an east-west elongation of $\simeq 2''$, but a similar shape is seen in a nearby source (Fig. 3). We conclude that the source is unresolved. It lies within $\simeq 0''.5$ of the radio continuum position for L1551 NE A found by Reipurth et al. (2002b). Preliminary X-ray properties of L1551 NE are as follows: 40 events with a distinctly hard spectrum extending to 7 keV, with soft energy cutoff around 2.0–2.5 keV. This implies $\log N_{\text{H}} \sim 22.0\text{--}23.0 \text{ cm}^{-2}$, or $A_{\text{V}} \simeq$ tens, consistent with an origin from the protostar itself. Photon arrivals do not appear to be constant, with higher fluxes at the beginning and end of the observation compared to the middle. Probability of constancy is $P = 0.004$, equivalent to 3σ , from a one-sample Kolmogorov-Smirnov test.

4. MODELS FOR THE X-RAY SOURCE ASSOCIATED WITH IRS 5

In this section, we discuss the source of the X-rays from the vicinity of L1551 IRS 5. As discussed above, it is unlikely that one or both members of this protobinary can be seen directly at soft X-ray wavelengths because of the

high foreground column density. Furthermore, the X-ray source near IRS 5 has the following properties. First, the X-ray source is displaced by $0''.5\text{--}1''$ from the position of L1551 IRS 5 toward the blueshifted lobe of the protostellar outflow. Second, the X-ray emission is slightly extended along the HH 154 jet axis. Third, the low-energy cutoff in the X-ray spectrum indicates that the source is attenuated by a considerably lower column of foreground material than the column responsible for hiding L1551 IRS 5 at visual and near-IR wavelengths. All of these observed properties make a direct association with IRS 5 unlikely.

The properties of L1551 source 31 can be compared with the X-ray emission from knot 2H in HH 2, observed with *Chandra* ACIS by Pravdo et al. (2001). In HH 2, the X-ray emission coincides with a high-excitation shock (to within less than $0''.5$) bright in species such as [O III]. This knot has a large proper motion (Bally et al. 2002) and is the brightest nonstellar radio continuum source in the HH 1/2 outflow. The X-ray emission is resolved, with an extent of $2''$, or ~ 1000 AU, and has a soft spectrum with temperature $T \simeq 1$ MK.

4.1. Infrared Emission from the HH 154 Jet

The $1.644\ \mu\text{m}$ [Fe II] spectrum of Pyo et al. (2002) shows that the inner $5''$ of the northern jet emerging from IRS 5 has two velocity components: a low-velocity component with a radial velocity of $v_{\text{LSR}} \approx -100\ \text{km s}^{-1}$, which peaks at the location of the [Fe II] knot PHK1 about $1''.5$ from IRS 5, and a high-velocity component with a radial velocity of $v_{\text{LSR}} \approx -300\ \text{km s}^{-1}$, which peaks at the location of knot PHK2 about $4''.5$ from IRS 5. The FWHM widths of these emission components are about 130–160 and 40 km s^{-1} for the slow and fast components, respectively. However, in the Pyo et al. (2002) position-velocity diagrams, faint emission can be traced from near -50 to $-350\ \text{km s}^{-1}$ from within $1''$ to more than $4''.5$ from IRS 5. The faint high-velocity emission that first appears near PHK1 grows in intensity with increasing distance from IRS 5 and dominates the low-velocity component beyond $2''$ from IRS 5. Visual-wavelength emission lines also show the presence of several velocity components in HH 154 (Stoche et al. 1988; Hartigan et al. 2000). Because the flow is inclined by about 45° with respect to the plane of the sky, the true space velocities are about a factor of 1.4 higher.

From the astrometric registration to other sources (bright stars, HL and XZ Tau, and L1551 NE), the X-ray source appears to be located $0''.5\text{--}1''$ west-southwest of the VLA position for IRS 5. The most likely association with a feature in the HH 154 jet is the bright [Fe II] knot PHK1 (Pyo et al. 2002). Although [Fe II] emission from this feature is dominated by gas with a radial velocity of about $-100\ \text{km s}^{-1}$, there is also some weak high-velocity emission, with radial velocities extending to $-350\ \text{km s}^{-1}$. The deprojected flow velocity in the fast component of the [Fe II] emission is greater than $500\ \text{km s}^{-1}$.

Figure 4 shows the relative locations of the protostars and the X-ray source superimposed on an optical image of the HH 154 jet obtained in 2001 October with the MOSAIC CCD camera on the Mayall 4 m reflector at KPNO. This image shows the sum of the emission observed in $80\ \text{\AA}$ pass-band interference filters centered on the $\text{H}\alpha$ and [S II] emission lines. In the following, we consider several alternative models for the X-ray source associated with HH 154.

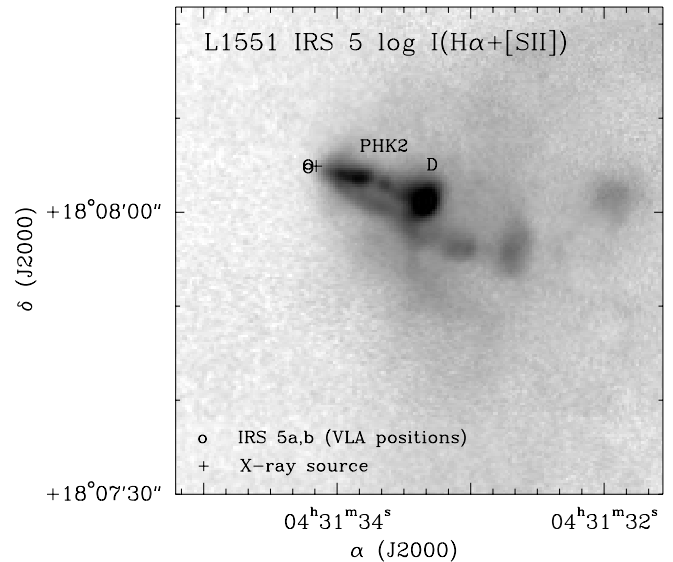


FIG. 4.—Location of the VLA source, X-ray source 31, superimposed on an optical image of the HH 154 jet. The optical image shows the sum of $\text{H}\alpha$ and [S II] images obtained through $80\ \text{\AA}$ passband filters with the KPNO 4 m Mayall reflector.

4.2. X-Rays Scattered from IRS 5?

Seyfert 2 galaxies show a spectral component that is scattered into the line of sight by a “warm scattering medium” located above the disk or torus that obscures the central engine from view (Matt, Brandt, & Fabian 1996; Bianchi & Matt 2002). It is possible that X-rays produced by IRS 5 are reflected into our line of sight by such a scattering layer located about 200 AU from the protostar.

Since only 0.5–5 keV X-rays are observed from IRS 5 (see § 3.1), Thompson scattering will dominate over other processes. If the X-ray intrinsic luminosity of the protostar is L_p and the scattering medium subtends an angle Ω as seen from the YSO, the reflected X-ray luminosity L_X is

$$\frac{L_X}{L_p} \approx \frac{\Omega\tau}{4\pi},$$

where τ is the opacity of the scattering medium (assumed to be less than 1). Assuming a protostellar X-ray luminosity of $L_p = 10^{29}\ \text{ergs s}^{-1}$, Ω and τ must be close to or larger than 1 sr and unity, respectively, to get the observed X-ray luminosity of HH 154. For a scattering screen depth of L (about 100 AU), the required density is $n_e \approx 1/\sigma_T L\tau$, where $\sigma_T = 6.65 \times 10^{-25}\ \text{cm}^2$ is the Thomson cross section. For $\tau = 1$, $n_e \approx 10^9\ \text{cm}^{-3}$. Such high electron densities are not likely to be found in a jet, but might exist in the circumstellar disk or in an infalling envelope.

If the scattering medium were ionized, it ought to be very bright in the radio continuum and in $\text{H}\alpha$. To produce a significant X-ray reflection from a hidden source requires an electron column density of $N_e = n_e L \approx \tau/\sigma_T \sim 10^{24}\ \text{cm}^{-2}$ confined to a region with an extent $L \sim 10^{15}\ \text{cm}$. The implied emission measure, $n_e^2 L = 3 \times 10^{14}\ \text{cm}^{-6}\ \text{pc}$, and the source size would produce an opaque radio continuum source many orders of magnitude brighter than any observed near L1551 IRS 5. But if the plasma cloud were significantly smaller and still located roughly $10^{15}\ \text{cm}$ from the source, Ω would be too small to reflect enough X-rays.

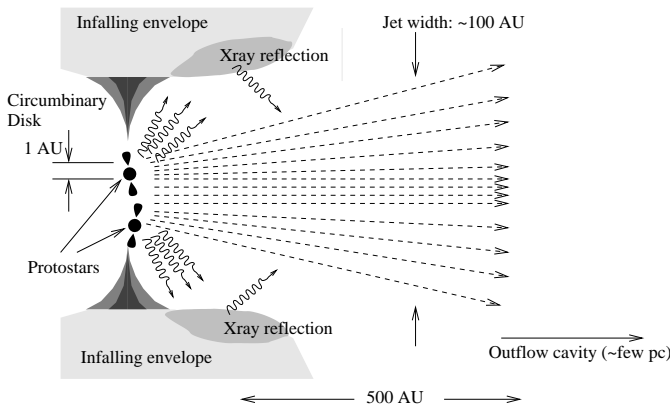


FIG. 5.—Cartoon showing one possible geometry, in which a dense medium reflects stellar magnetospheric X-rays into the line of sight. The jet axis is inclined toward our line of sight by about 45° . In this model, the low-velocity [Fe II] component may be produced by either interactions of the jet with the surrounding medium or illumination from the embedded young stars. The high-velocity near-infrared [Fe II] emission must be produced by internal shocks in the jet beam.

Furthermore, the recombination rate in the plasma is roughly given by $L^3 n_e^2 \alpha_B \sim 10^{50} \text{ s}^{-1}$, where $\alpha_B = 2.6 \times 10^{-13} \text{ cm}^6 \text{ s}^{-1}$ is the recombination rate for hydrogen at 10^4 K . To maintain the plasma requires an ionization rate many orders of magnitude higher than plausible near a low-mass protostar. Thus, we conclude that any scattering medium must be mostly neutral.

Electrons in bound states can also scatter X-rays. The above length scale and density imply that the mass of the scattering medium is of the order of $M = \mu m_H n_H L^3 \sim 10^{-3} L_{15} n_9 M_\odot$, where L_{15} is the size of the region in units of 10^{15} cm , n_9 is the hydrogen density in units of 10^9 cm^{-3} , $\mu = 1.4$ is the mean molecular weight, and m_H is the mass of a hydrogen atom. If this medium were part of the neutral wind emerging from L1551 IRS 5, the implied mass-loss rate is $\dot{M} = Mv/L \approx 4 \times 10^{-4} L_{15}^{-1} v_{100} M_\odot \text{ yr}^{-1}$, where v_{100} is the flow speed in units of 100 km s^{-1} . Such a high mass-loss rate is plausible and may occur if the source is in an FU Ori outburst. However, the requirement that the scattering layer subtends about 1 sr as seen from the source implies that any such flow must be a wide-angle wind and not a collimated jet.

An alternative possibility is that the scattering occurs in an accreting envelope. The infall speed is given roughly by the escape speed at the characteristic distance from the star, about $v_{\text{esc}} = (GM/L)^{1/2} \approx 3.6 \text{ km s}^{-1}$ for a $1 M_\odot$ star at $L = 10^{15} \text{ cm}$. The implied mass accretion rate is $\dot{M} = Mv_{\text{esc}}/L \approx 1.5 \times 10^{-5} L_{15}^{-1} v_4 M_\odot \text{ yr}^{-1}$, where v_4 is the infall speed in units of 4 km s^{-1} , not atypical for class 0 and extreme class I protostars.

Figure 5 shows one possible geometry, in which X-rays from IRS 5 might be scattered into our line of sight by a dense medium. In this scenario, the scattering layer is probably associated with the inner edge of the circumbinary disk.

4.3. Comoving Shocks in the HH 154 Jet

Observations of protostellar jets, such as HH 1/2, 34, 111, and 46/47, indicate that within about 10^{17} cm of the source, the jet is made visible by low-excitation bow shocks within the flow. These are likely produced by small-

amplitude velocity variations superimposed on the bulk motion of the flow (Dopita 1978a, 1978b; Raga et al. 1990; Stone & Norman 1993a, 1993b; Hartigan et al. 2001; Bally et al. 2002). This emission is dominated by first ionization stage or neutral species such as [Fe II], [O I], and [S II], indicating internal shock speeds of $20\text{--}60 \text{ km s}^{-1}$ and postshock temperatures of the order of 10^4 K . Proper-motion measurements demonstrate that these “internal working surfaces” move with the bulk flow with speeds of $200\text{--}400 \text{ km s}^{-1}$. These low-amplitude internal velocity variations render classical HH jets visible.

Favata et al. (2002) argue that the X-ray emission from HH 154 is associated with knot D, located about $5''$ from IRS 5. Our significantly improved position for the X-ray source indicates that the X-ray source is probably associated with knot PHK1 at the base of the HH 154 jet. As shown further below, it is unlikely that internal working surfaces in the jet beam can produce plasmas with a sufficiently high temperature to produce the observed X-rays.

4.4. X-Rays from Fast Shocks

It is possible that the X-ray source near IRS 5 traces emission produced by fast shocks where the protostellar wind encounters an obstacle. The postshock temperature in the adiabatic (nonradiative) portion of a shock is given by

$$T_{\text{ps}} = \frac{2.9 \times 10^5}{1 + X} V_{100}^2 \text{ K}$$

(Ostriker & McKee 1988), where V_{100} is the velocity of the shock front with respect to the downstream material (the shock velocity) in units of 100 km s^{-1} and X is the ionization fraction of the preshock gas ($X = 0$ for a neutral medium and 1 for a fully ionized one). Thus, a plasma temperature of $4 \times 10^6 \text{ K}$ (Favata et al. 2002) requires a shock speed of 371 km s^{-1} for a shock moving into a mostly neutral medium, or 525 km s^{-1} for a shock moving into a fully ionized medium. These speeds are comparable to the deprojected space velocities of the fast component in HH 154. Our estimated plasma temperature of 10^7 K requires a 590 km s^{-1} shock propagating into a neutral medium.

The expected X-ray luminosity, L_X , of a shock-heated source depends on the emissivity per unit volume, which depends on the temperature and density, the volume of the emitting region, and the type of shock—radiative or nonradiative (Raga, Noriega-Crespo, & Velázquez 2002). For a radiative shock, they find

$$L_r = 4.1 \times 10^{-6} n_{100} r_{16}^2 V_{100}^{5.5} L_\odot$$

and for a nonradiative shock

$$L_{\text{nr}} = 4.5 \times 10^{-5} n_{100}^2 r_{16}^3 V_{100} L_\odot,$$

where n_{100} is the preshock density in units of 100 cm^{-3} and r_{16} is the radius of the jet or object driving the shock in units of 10^{16} cm . The *HST* observations of the HH 154 jet (Fridlund & Liseau 1998) show that near its base, the jet has a radius of about $0''.5$, or about $1.05 \times 10^{15} \text{ cm}$. Using a shock speed of 400 km s^{-1} (a lower bound based on the Favata et al. 2002 results), this dimension for the X-ray source and a preshock density of 500 cm^{-3} imply $L_r = 4.6 \times 10^{-4} L_\odot = 1.9 \times 10^{30} \text{ ergs s}^{-1}$, or $L_{\text{nr}} = 5.2 \times 10^{-6} L_\odot = 2.1 \times 10^{28} \text{ ergs s}^{-1}$. Thus, a flow with a reasonable density can readily explain the X-ray luminosity. But, what is the shock

geometry and where is it located? In the next subsections three possibilities are discussed.

4.4.1. Shocks Associated with Jet Collimation

Both X-wind and disk-wind models (see, e.g., Shu et al. 2000) accelerate outflows within a few AU of a protostar. Near their points of origin, outflows can have opening angles of 10° – 60° and spread to a width of around 100 AU before being collimated into a jet. The *HST* observations of the HH 154 jet (Fridlund & Liseau 1998) show that by the time the outflow emerges a few hundred AU from the source, it has become collimated into a jet with a transverse extent of at least 50 AU.

Collimation requires a dense medium and/or magnetic hoop stress that can redirect the flow. In either scenario, the abrupt reorientation of the flow shocks the diverging wind; the \mathbf{B} -field or dense medium acts like a nozzle that produces quasi-stationary shocks in which the shock velocity will be comparable to the flow speed (Gomez de Castro & Pudritz 1993). It is possible that the low-velocity [Fe II] emission is produced by shocks propagating into the medium responsible for jet collimation, while the X-ray emission traces the quasi-stationary shock where the fast wind from the protostar is collimated into a jet. The wind enters with a shock velocity given by $v_s = v_w \cos i$, where i is the angle between the shock normal and the direction of the flow entering the shock and v_w is the wind speed. Figure 6 shows a possible geometry for the collimation shock.

Why does the X-ray source coincide with knot PHK1, which is dominated by low radial velocity emission, and not PHK2, which is dominated by high radial velocity emission? A possible explanation is that the two fluids colliding at PHK1 have different densities. The X-rays may be produced by a reverse shock, into which the fast wind is flowing. The $v_{\text{LSR}} = -100 \text{ km s}^{-1}$ [Fe II] component may originate behind a shock moving into a denser medium, which may be located just outside the region occupied by the fast flow. This medium may be stationary or moving slowly. It could be associated with the infalling envelope or the dense gas above the circumbinary disk, or it may even be part of a lower velocity disk wind.

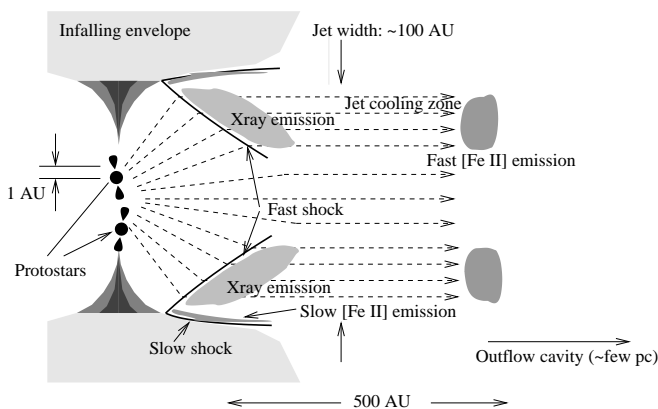


FIG. 6.—Cartoon showing one possible geometry for a strong shock that could produce the observed X-ray emission at the base of the HH 154 jet. The jet axis is inclined toward our line of sight by about 45° . In this model, the low-velocity near-infrared [Fe II] emission is produced by the slow shocks propagating into the collimating medium, and the high-velocity [Fe II] emission traces the cooling layer downstream from the X-ray-luminous fast shocks.

The total internal pressure (thermal and ram, plus magnetic) in the collimating medium must be greater than the ram pressure of the wind. Assuming an initial opening angle of 45° and the above jet density and flow speed implies $P/k = (2\text{--}20) \times 10^9 \text{ cm}^{-3} \text{ K}$. For a 10^4 K medium (implied by the [Fe II] emission), the density in the collimating medium must be of the order of 10^6 cm^{-3} if the magnetic field or ram pressure is small. If static magnetic pressure dominates, then the implied field strength is around 1–4 mG. However, it is possible that this medium is also in motion, because it is part of either a disk wind or an infalling envelope. Furthermore, it is possible that the thermal, ram, and magnetic pressures are in rough equipartition, in which case the densities and implied magnetic fields may be lower.

4.4.2. Shocks Produced by Wind-Disk Collisions

In a binary system, if the individual circumstellar disks and/or the circumbinary disk are not coplanar, the jet or wind from one protostar may impact either the other circumstellar disk or the circumbinary disk. The resulting collision might produce a standing shock. In the case of L1551 IRS 5, the location of the X-ray source seems to rule out a shock associated with one of the circumstellar disks. But the interaction could occur with a portion of the circumbinary disk. Such an interaction requires that the circumbinary disk have an inclination different from that of the circumstellar disk producing the outflow; in L1551, the circumbinary disk would have to lie nearly in the plane of the sky to get into the path of the southwest-moving flow. This configuration is considered unlikely, since on large scales the circumbinary material appears to be elongated orthogonal to the outflow axis (see, e.g., Hogerheijde et al. 1998; Fridlund et al. 2002). This model is similar to the one shown in Figure 6, except that the interaction would occur predominantly at one location along the inner edge of the circumbinary disk and therefore would not be as symmetric as the collimation shock shown in Figure 6.

4.4.3. Shocks Produced by Wind-Wind Collisions

L1551 IRS 5 is a binary with a projected separation of about 40 AU. Fridlund & Liseau (1998) show that two jets are emerging from this region. Thus, it is possible that both protostars are powering stellar winds, which are colliding near the base of the jet. The shock parameters in this scenario are similar to those discussed above. The main difference is that rather than being located along the walls of the outflow cavity, the X-ray-producing shocks are likely to be near the center. Instead of shocking against a dense, nearly stationary medium, the wind shocks against the wind from the companion star. Figure 7 shows the geometry of shocks produced by wind-wind collisions. As is the case for a jet collimation shock, the shock is a quasi-stationary structure, and the wind enters with a shock velocity given by $v_s = v_w \cos i$. In this scenario, the low-velocity [Fe II] emission is probably unrelated to the X-ray emission; it may be produced where the wind rams the surrounding medium. As shown below, the fast [Fe II] emission may be produced in the postshock cooling layer downstream from the X-ray emission region.

4.5. The Cooling of the Postshock Medium

The high plasma temperature in the postshock region where the X-rays are produced precludes strong visual or

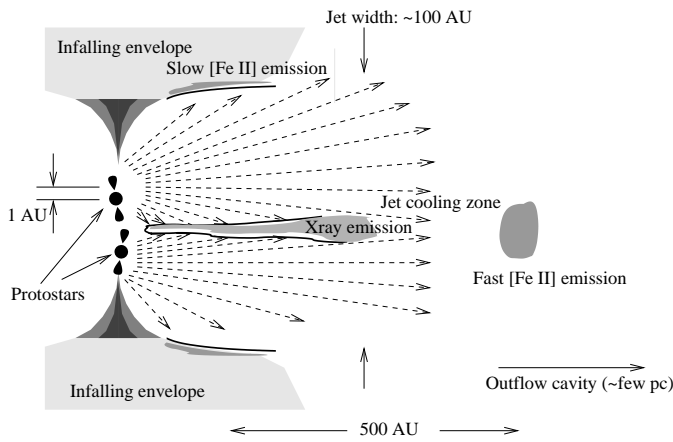


FIG. 7.—Cartoon showing a second possible geometry for a strong shock formed where winds from both members of the IRS 5 binary collide. The jet axis is inclined toward our line of sight by about 45° . In this model, the low-velocity near-infrared [Fe II] emission is produced by slow shocks propagating into the circumbinary disk. The high-velocity [Fe II] emission traces the cooling layer downstream from the X-ray-luminous fast shocks.

near-infrared wavelength forbidden-line emission, since most species will be in high ionization states. Emission from low ionization states should only appear downstream in the main body of the jet after it has had a chance to cool to under 10^5 K, at which point low ionization states become abundant. Thus, high-velocity [Fe II] emission is at first expected to be very faint. The brightness of this tracer is expected to increase downstream as the abundance of Fe II increases with decreasing temperature.

In the context of either the jet collimation shock, jet-disk collision, or colliding-wind models, it is possible that the brightening fast component of the [Fe II] emission between PHK1 and PHK2 traces this postshock cooling zone. The current separation between the two peaks is about $4''$, or 560 AU, in projection; the true separation is about 800 AU ($=1.2 \times 10^{16}$ cm). At a speed of 600 km s^{-1} , this distance is traversed in only 6 yr. If the bright part of the jet between the knots PHK1 and PHK2 corresponds to the cooling length, then the cooling time is in the range 2–10 yr. Using the interpolation formula for the cooling length from Heathcote, Reipurth, & Raga (1998), this cooling length implies a preshock density $n_{\text{H}} \approx (1-10) \times 10^3 \text{ cm}^{-3}$ in the flow, a very reasonable value that agrees with the preshock density required to explain the X-ray emission.

The long-term variations in the X-ray emission from the source near IRS 5 are consistent with a variable outflow ejection history. When the first *ROSAT* observations of this region were taken in 1993, the material now producing PHK1 had not yet been launched. If energized by a 600 km s^{-1} flow, the dynamical age of PHK1 is only a few years. Thus, either fast-shock model is expected to produce X-ray emission that varies on a timescale of years.

5. CONCLUSIONS

The first results of a 79 ks observation of 0.5–8 keV X-rays from the L1551 star-forming region, obtained with *Chandra*, are presented. The new data demonstrate that the X-ray source detected by Favata et al. (2002) and interpreted by them as arising from knot D in the HH 154 jet emerging from L1551 IRS 5 is actually a compact source

located at the *base* of the jet near knot PHK1. It is unlikely that this source is associated with IRS 5 itself, for several reasons. First, the X-ray source is displaced from IRS 5 by $0''.5-1''$ to the southwest along the jet axis. Second, IRS 5 is deeply embedded in circumstellar matter; the X-ray spectrum is inconsistent with the column density of foreground material required to obscure IRS 5. In addition, the X-ray source appears to be marginally resolved, with an extension along the jet axis; its location coincides with a bright knot of [Fe II] emission at the base of the HH 154 protostellar jet. The spectroscopic study of Pyo et al. (2002) demonstrates that knot PHK1 at the base of the HH 154 jet consists of predominantly low radial velocity [Fe II] emission, with $v_{\text{LSR}} \approx -100 \text{ km s}^{-1}$. However, a fast component of [Fe II] emission $v_{\text{LSR}} \approx -350 \text{ km s}^{-1}$ first appears at this location and gets brighter downstream.

In this paper, various models for the X-ray emission from L1551 IRS 5 are considered. The first possibility is that a dense medium within about 100 AU of the protobinary is reflecting X-rays from one or both protostars. The medium must subtend about 1 sr as seen from the source, have a density around 10^9 cm^{-3} , and be mostly neutral. If this scattering screen is located about 10^{15} cm from the source, as indicated by astrometry, and is about 10^{15} cm in extent, the mass of the medium must be about $0.001 M_{\odot}$. If this medium is associated with the outflow, the implied mass-loss rate must be about $\dot{M} \approx 4 \times 10^{-4} L_{15}^{-1} v_{100} M_{\odot} \text{ yr}^{-1}$ and the flow must be in the form of a wide-angle wind. If the medium is either orbiting the star or, more likely, infalling at the local escape speed, then the implied mass accretion rate is about $\dot{M} \approx 1.5 \times 10^{-5} L_{15}^{-1} v_4 M_{\odot} \text{ yr}^{-1}$.

A more attractive model is one in which the X-ray source traces a fast shock at the base of the HH 154 jet, where a wide-angle flow, launched and accelerated within a few AU of one member of the IRS 5 protobinary, is redirected and collimated into a jet. The jet shock model of Raga et al. (2002) indicates that the 10^7 K plasma implied by the X-ray data requires a shock velocity of at least 590 km s^{-1} . The excitation conditions, radial velocity, and proper-motion studies of the velocity difference between pre- and postshock gas indicate that most Herbig-Haro jets have internal working surfaces with shock speeds nearly an order of magnitude lower. The collimation shock where a faster than 350 km s^{-1} flow is redirected is a plausible environment in which a shock of sufficient speed to produce the X-ray emission can exist. In this model, the X-ray emission arises from the hot layer downstream from a quasi-stationary shock. For an assumed jet diameter of 70 AU, the X-ray luminosity requires a radiative shock with a shock velocity greater than 350 km s^{-1} and a preshock density larger than 500 cm^{-3} .

We also consider two variations of this model. In one, the outflow may slam into a portion of the circumbinary disk. However, this requires a nearly face-on disk, an unlikely circumstance. In the other, the X-ray source is powered by the collision of a pair of stellar winds emerging from the IRS 5 binary system. The shock parameters of this model are similar to those involving the collimation shock. However, the geometry is completely different. A collimation shock would be located near the outer rim of the outflow cavity, while a wind-wind collision shock should be located inside the cavity where the flows collide.

The high-velocity [Fe II] feature that first appears near the X-ray knot close to the position of PHK1, but becomes bright near PHK2, may trace the cooling length in the

plasma in either fast-shock model. The low-velocity [Fe II] component in PHK1 may trace shocks propagating into the dense circumstellar environment in the collimation shock or disk-wind collision model. This feature does not find a natural explanation in the wind-wind collision scenario.

There is excellent agreement between the cooling time in the shock model for the X-ray source and the observed length of the HH 154 jet. If the separation between knots PHK1 and PHK2, located about 4'' (560 AU in projection) downstream, corresponds to the cooling length of the fast fluid component, then the implied preshock density is about $(1-10) \times 10^3 \text{ cm}^{-3}$, close to the value derived from the X-ray luminosity. The absence of X-ray flaring during the observations but the possible presence of long-term flux variations indicated by previous nondetections of this source is

readily explained by the mass-loss rate and flow speed variations thought to be responsible for internal working surfaces in jets. Further modeling and observations are required to distinguish which model for the X-ray emission near L1551 IRS 5 is likely to be correct.

We thank Patrick Broos, Konstantin Getman, and especially Leisa Townsley (Penn State) for their expert and invaluable assistance in the *Chandra* data analysis, and Pat Hartigan, George Herbig, and Alex Raga for valuable suggestions. We also thank an anonymous referee for very useful comments. This research was supported by the *Chandra* X-Ray Science Center and NASA through ASO grant GO1-2004X. J. B. and B. R. acknowledge support from NASA grant NAG 5-8108 (LTSA).

REFERENCES

- Bally, J., Heathcote, S., Reipurth, B., Morse, J., Hartigan, P., & Schwartz, R. 2002, *AJ*, 123, 2627
- Bianchi, S., & Matt, G. 2002, *A&A*, 387, 76
- Campana, S., Gastaldello, F., Stella, L., Israel, G. L., Colpi, M., Pizzolato, F., Orlandini, M., & Dal Fiume, D. 2001a, *ApJ*, 561, 924
- Campana, S., Moretti, A., Lazzati, D., & Tagliaferri, G. 2001b, *ApJ*, 560, L19
- Carkner, L., Feigelson, E. D., Koyama, K., Montmerle, T., & Reid, I. N. 1996, *ApJ*, 464, 286
- Davis, C. J., Stern, L., Ray, T. P., & Chrysostomou, A. 2002, *A&A*, 382, 1021
- Devine, D., Bally, J., Reipurth, B., Stocke, J., & Morse, J. 2000, *ApJ*, 540, L57
- Devine, D., Reipurth, B., & Bally, J. 1999, *AJ*, 118, 972
- Dopita, M. A. 1978a, *ApJS*, 37, 117
- . 1978b, *A&A*, 63, 237
- Favata, F., Fridlund, C. V. M., Micela, G., Sciortino, S., & Kaas, A. A. 2002, *A&A*, 386, 204
- Feigelson, E. D., Broos, P., Gaffney, J. A., III, Garmire, G., Hillenbrand, L. A., Pravdo, S. H., Townsley, L., & Tsuboi, Y. 2002, *ApJ*, 574, 258
- Feigelson, E. D., & DeCampli, W. M. 1981, *ApJ*, 243, L89
- Feigelson, E. D., & Kriss, G. A. 1981, *ApJ*, 248, L35
- Freeman, P. E., Kashyap, V., Rosner, R., & Lamb, D. Q. 2002, *ApJS*, 138, 185
- Fridlund, C. V. M., Bergman, P., White, G. J., Pilbratt, G. L., & Tauber, J. A. 2002, *A&A*, 382, 573
- Fridlund, C. V. M., & Liseau, R. 1998, *ApJ*, 499, L75
- Getman, K. V., Feigelson, E. D., Townsley, L., Bally, J., Lada, C. J., & Reipurth, B. 2002, *ApJ*, 575, 354
- Gezari, D. Y., Pitts, P. S., & Schmitz, M. 1999, *Catalog of Infrared Observations* (5th ed.; Strasbourg: CDS)
- Gomez de Castro, A. I., & Pudritz, R. E. 1993, *ApJ*, 409, 748
- Hartigan, P., Morse, J., Palunas, P., Bally, J., & Devine, D. 2000, *AJ*, 119, 1872
- Hartigan, P., Morse, J. A., Reipurth, B., Heathcote, S., & Bally, J. 2001, *ApJ*, 559, L157
- Heathcote, S., Reipurth, B., & Raga, A. C. 1998, *AJ*, 116, 1940
- Hogerheijde, M. R., van Dishoeck, E. F., Blake, G. A., & van Langevelde, H. J. 1998, *ApJ*, 502, 315
- Matt, G., Brandt, W. N., & Fabian, A. C. 1996, *MNRAS*, 280, 823
- Mewe, R., Lemen, J. R., & van den Oord, G. H. J. 1986, *A&AS*, 65, 511
- Moriarty-Schieven, G. H., & Snell, R. L. 1988, *ApJ*, 332, 364
- Morrison, R., & McCammon, D. 1983, *ApJ*, 270, 119
- Mundt, R., Walter, F. M., Feigelson, E. D., Finkenzeller, U., Herbig, G. H., & Odell, A. P. 1983, *ApJ*, 269, 229
- Ostriker, J. P., & McKee, C. F. 1988, *Rev. Mod. Phys.*, 60, 1
- Pravdo, S. H., Feigelson, E. D., Garmire, G., Maeda, Y., Tsuboi, Y., & Bally, J. 2001, *Nature*, 413, 708
- Pyo, T.-S., Hayashi, M., Kobayashi, N., Terada, H., Goto, M., Yamashita, T., Tokunaga, A. T., & Itoh, Y. 2002, *ApJ*, 570, 724
- Raga, A. C., Cantó, J., Binette, L., & Calvet, N. 1990, *ApJ*, 364, 601
- Raga, A. C., Mundt, R., & Ray, T. P. 1991, *A&A*, 252, 733
- Raga, A. C., Noriega-Crespo, A., & Velázquez, P. F. 2002, *ApJ*, 576, L149
- Ray, T. P., Mundt, R., Dyson, J. E., Falle, S. A. E. G., & Raga, A. C. 1996, *ApJ*, 468, L103
- Reipurth, B. 1999, *A General Catalogue of Herbig-Haro Objects* (2d ed.; Boulder: CASA)
- Reipurth, B., Heathcote, S., Morse, J., Hartigan, P., & Bally, J. 2002a, *AJ*, 123, 362
- Reipurth, B., Lindgren, H., Nordström, B., & Mayor, M. 1990, *A&A*, 235, 197
- Reipurth, B., Rodríguez, L. F., Anglada, G., & Bally, J. 2002b, *AJ*, 124, 1045
- Reipurth, B., Yu, K. C., Heathcote, S., Bally, J., & Rodríguez, L. F. 2000, *AJ*, 120, 1449
- Rodríguez, L. F., et al. 1998, *Nature*, 395, 355
- Shu, F. H., Najita, J. R., Shang, H., & Li, Z.-Y. 2000, in *Protostars and Planets IV*, ed. V. Mannings, A. P. Boss, & S. S. Russell (Tucson: Univ. Arizona Press), 789
- Snell, R. L., Loren, R. B., & Plambeck, R. L. 1980, *ApJ*, 239, L17
- Stocke, J. T., Hartigan, P. M., Strom, S. E., Strom, K. M., Anderson, E. R., Hartmann, L. W., & Kenyon, S. J. 1988, *ApJS*, 68, 229
- Stone, J. M., & Norman, M. L. 1993a, *ApJ*, 413, 198
- . 1993b, *ApJ*, 413, 210
- Townsley, L. K., Broos, P. S., Chartas, G., Moskalenko, E., Nousek, J. A., & Pavlov, G. G. 2002, *Nucl. Instrum. Methods Phys. Res. A*, 486, 716
- Townsley, L. K., Broos, P. S., Garmire, G. P., & Nousek, J. A. 2000, *ApJ*, 534, L139
- Weisskopf, M. C., Brinkman, B., Canizares, C., Garmire, G., Murray, S., & Van Speybroeck, L. P. 2002, *PASP*, 114, 1
- Wendker, H. J. 1995, *A&AS*, 109, 177
- White, G. J., et al. 2000, *A&A*, 364, 741